ELSEVIER

Journal of Structural Geology 30 (2008) 513–524

JOURNAL OF STRUCTURAL GEOLOGY

www.elsevier.com/locate/jsg

Internal structure and permeability of the Nojima fault, southwest Japan

Kazuo Mizoguchi [a,*], Takehiro Hirose [b], Toshihiko Shimamoto [c], Eiichi Fukuyama [a]

[a] Earthquake Research Department, National Research Institute for Earth Science and Disaster Prevention, 3-1 Tenno-dai, Tsukuba, Ibaraki 305-0006, Japan
[b] Kochi Institute for Core Sample Research, Japan Agency for Marine-Earth Science and Technology (JAMSTEC), Kochi 783-8502, Japan
[c] Department of Earth and Planetary Systems Science, Hiroshima University, Higashi-Hiroshima 739-8526, Japan

Received 2 March 2007; received in revised form 23 November 2007; accepted 2 December 2007
Available online 15 December 2007

Abstract

We conducted permeability measurements on representative fault rocks and surrounding country rocks taken from the Nojima fault zone, which was activated during the 1995 Kobe earthquake, under isotropic confining pressures up to 180 MPa. The results show that the Nojima fault zone consists of a low-permeability fault gouge zone (10^{-20}–10^{-19} m^2 at 180 MPa) within a high-permeability damaged zone of fault breccia and fractured host rock (10^{-18}–10^{-14} m^2 at 180 MPa). The fault gouge zone acts as a barrier to fluid flow across the fault, whereas the surrounding damage zone acts as a fluid conduit. The nature of this proposed permeability structure is consistent with the results of tests conducted on drillcore samples collected from the Nojima fault at depths of 0.6 and 1.8 km. We therefore propose that the permeability of a fault measured from fault rocks exposed at the surface can be used as a representative value for the fault to depths of up to 2 km. We also examined the possibility that thermal pressurization occurred upon the Nojima fault during the Kobe earthquake, based on the obtained permeability data. We found that frictional heating during the Kobe earthquake would have led to an increase in pore pressure at depths below 4 km, thereby resulting in a marked reduction in frictional resistance upon the fault.

Keywords: Nojima fault; Permeability; Surface samples; Thermal pressurization

1. Introduction

Permeability is one of the key hydraulic parameters in modeling fluid flow in rocks. The permeability of crystalline and sedimentary rocks has been measured intensively for nearly a century (Schön, 1996), and data have recently been reported for fault-related rocks found along natural faults (Evans et al., 1997; Seront et al., 1998; Kitagawa et al., 1999; Lockner et al., 2000; Wibberley and Shimamoto, 2003; Tsutsumi et al., 2004; Uehara and Shimamoto, 2004). The influence of fluids (e.g., water) upon fault behavior is closely related to seismic activity (Healy et al., 1968; Ohtake, 1974; Zoback and Harjes, 1997) and thermal pressurization associated with seismic fault motion (Sibson, 1973; Lachenbruch, 1980; Mase and Smith, 1985, 1987). Recent analyses of thermal pressurization based on permeability data from natural faults (Noda and Shimamoto, 2005; Wibberley and Shimamoto, 2005; Bizzarri and Cocco, 2006a,b; Rice, 2006) have attracted great interest because the mechanism is able to explain the dynamic weakening behavior of faults observed during earthquakes; this behavior is not observed in laboratory-based friction experiments. Thus, it is of great importance to investigate the permeability structure of natural faults.

Permeability is typically measured using one of the following three methods: (1) *in situ* water-injection experiments using boreholes; (2) laboratory experiments on drillcore samples; and (3) laboratory experiments on samples collected from surface outcrops. *In situ* measurements provide permeability data under the ambient temperature and pressure conditions of the study site; however, in this case the obtained permeability represents the average value for the volume of rock that extends several hundred meters from the borehole. Thus, *in situ* measurements are of limited use in identifying the permeability structure of faults that possess a complex

* Corresponding author. Tel.: +81 29 863 7693; fax: +81 29 863 7610.
E-mail address: mizo@bosai.go.jp (K. Mizoguchi).

0191-8141/$ - see front matter © 2007 Elsevier Ltd. All rights reserved.
doi:10.1016/j.jsg.2007.12.002

internal structure consisting of, for example, a fault core, a damage zone, and the surrounding host rock (Caine et al., 1996); in such cases, laboratory-based experiments represent a more suitable approach.

To investigate the permeability of faults at depth, it is necessary to conduct permeability measurements using core samples obtained at depth; however, most measurements are performed using samples from surface outcrops because they are easily obtained at minimal cost. The use of surface samples makes it possible to conduct many experiments in precisely measuring the permeability properties under varying conditions of, for example, pressure, temperature, and deformation; however, it remains to be determined whether surface samples can be used to investigate the permeability structure of a fault at depth. Although a comparison of the permeability at the surface with that at depth has already been performed for crystalline rocks (Morrow and Lockner, 1994), such a study has yet to be undertaken for fault-related rocks.

In the present study, we describe the internal structure of the Nojima fault, Southwest Japan, as observed at two outcrops (Funaki and Hirabayashi; Fig. 1), and measure the permeability of fault-related rocks from these sites under high pressures and room temperatures.

The Nojima fault was activated during the 1995 Hyogo-ken Nanbu (Kobe) earthquake ($M = 7.2$), with a hypocenter depth of 16.0 km. After the earthquake, a drilling project was carried out to intersect the fault zone, and the permeability of the zone has since been measured via water injection tests within the boreholes (e.g., Kitagawa et al., 1999) and laboratory-based measurements of core samples (Lockner et al., 2000). Comparing our results with those of these previous studies, we are able to demonstrate the validity of the use of surface samples in inferring the nature of permeability structures within fault zones at depth. Based on the obtained permeability data, we also examine the possibility that thermal pressurization occurred upon the Nojima fault during the Kobe earthquake.

2. Geological setting

The 9-km-long Nojima fault, which strikes northeast-southwest and dips steeply to the southeast, runs along the northwestern margin of Awaji Island in Hyogo prefecture, Southwest Japan, and forms part of a 60-km-long belt of active faults known as the Rokko-Awaji fault system (e.g., Huzita, 1967, 1969) (Fig. 1). Geologically, the area in which the fault occurs consists of Cretaceous granite and granodiorite overlain by the Miocene Kobe Group (sand, conglomerate, and sandy mud) and the Plio-Pleistocene Osaka Group (silt-clay, sand, and conglomerate). The east side of the Nojima fault is upthrown, bringing granitic rocks into fault contact with the overlying sediments. The total Quaternary vertical displacement upon the Nojima fault is estimated to be about 500 m, as estimated from a vertical geological cross-section constructed from borehole data (Murata et al., 1998).

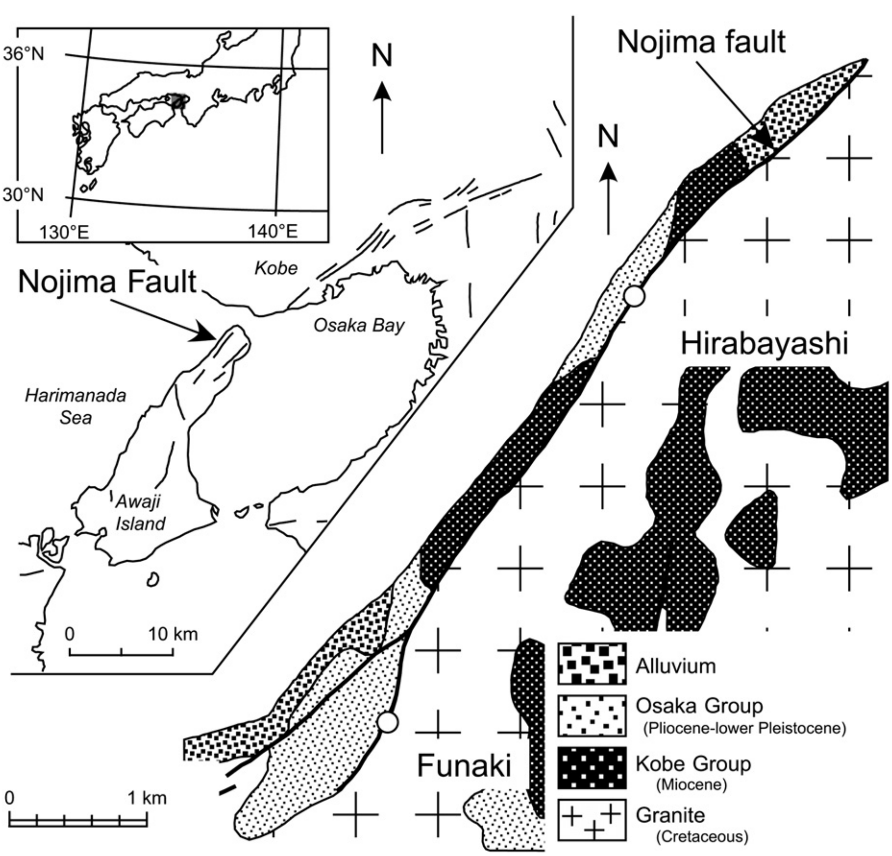

Fig. 1. Map of active faults upon Awaji Island and adjacent areas, and geological map along the trace of the Nojima fault (modified from Awata and Mizuno, 1998). The open circles show the locations sampled in the present study.

The outcrops of the Nojima fault analyzed in the present study are located at Hirabayashi and Funaki (Fig. 1). At Hirabayashi, surface fault ruptures associated with the 1995 Kobe earthquake record maximum right-lateral and vertical (reverse) displacements of 2.0 and 1.4 m, respectively (Awata and Mizuno, 1998). The surface fault rupture branched at Nashimoto, in the southwestern part of the fault. The branch fault terminates near Funaki, where horizontal and vertical displacements of 0.08 and 0.06 m were recorded, respectively.

3. Structure of the Nojima fault zone

3.1. Funaki outcrop

At Funaki, the southeast side the Nojima fault zone consists of a zone of fault gouge (about 0.1–0.15 m in width), a zone of fault breccia (about 2 m in width), and fractured granite host rock (Fig. 2). On the northwest side of the fault zone, conglomerate of the Osaka Group strikes parallel to the fault and dips at 40° to the west. Bedding planes within the conglomerate are offset along minor faults that contain injections of clayey gouge. The contact between the conglomerate and the gouge zone is highly irregular, and the contact between the gouge zone and the breccia zone is sharp and planar. The contact between the fault breccia zone and fractured granite is gradational.

The gouge zone is composed of weakly foliated greenish–gray clayey gouge (Fig. 3a). The structure of the host rock is completely obliterated within the gouge zone, and the texture is typically matrix-supported. Foliation is defined by the preferred orientation of clay minerals and color banding, with bands offset along Riedel shears that record a top-to-the-right sense of shear. The gouge contains angular to subangular fragments of quartz, alkali feldspar, and plagioclase of 0.05–0.25 mm in size. Matrix grains are dominated by quartz and clay minerals such as smectite and kaolinite.

The breccia zone consists of a granitic breccia part and a fine matrix part. The structure of the host rock is preserved at the mesoscopic scale in the granitic breccia part, but not in the matrix part. The microstructure of this zone is characterized by relatively large fragments of granite surrounded by a network of microfractures (Fig. 3b). The mesoscale density and width of microfractures within the breccia matrix are greater than those in the granitic breccia.

In the fractured granite, the structure of the host rock is intact, and intra- and intergranular cracks are prominent within mineral grains. The densities of the cracks and microfractures increase toward the fault.

The host rock, the Toshigawa granite, is composed mainly of quartz, plagioclase, and alkali feldspar, with subordinate hornblende and biotite. Intergranular cracks are rare in these grains (Mizuno et al., 1990) (Fig. 3d). Feldspar is milky white, quartz is relatively transparent, and grains of hornblende and biotite are scattered among larger crystals of quartz and feldspar.

Samples obtained for permeability measurements were collected from the fault gouge zone, the fault breccia zone, and the fractured granite zone within an excavated trench. Samples of fractured granite were also collected 10 m from the fault trace, and samples of fresh granite (host rock) were taken 100 m from the trace (see Table 1).

3.2. Hirabayashi outcrop

As with the outcrop at Funaki, the Nojima fault at Hirabayashi consists of three zones: a fault gouge zone (about 0.5–0.95 m in width), a fault breccia zone (about 2 m in width), and fractured granodioritic host rock (Fig. 4). Sandstone of the Osaka Group occurs on the northwest side of the fault. The fault gouge zone contains four types of fault gouge: a zone of brown gouge of about 0.05–0.8 m in width,

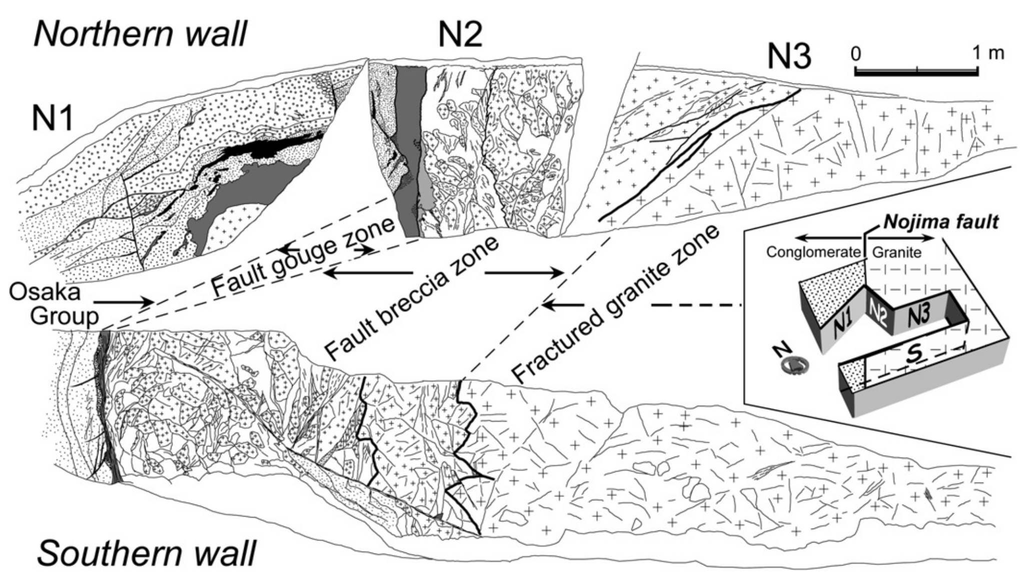

Fig. 2. Sketch of the northern (upper) and southern (down) walls in an excavation trench (see the block diagram to the right) at the Funaki site. The depth of the trench is about 2 m and the strike and dip of the faces are as follows: N1, N64E61S; N2, N23W50W; N3, N83W59S; S, N81W61S. The unmarked areas in the fault breccia zone are areas of breccia matrix.

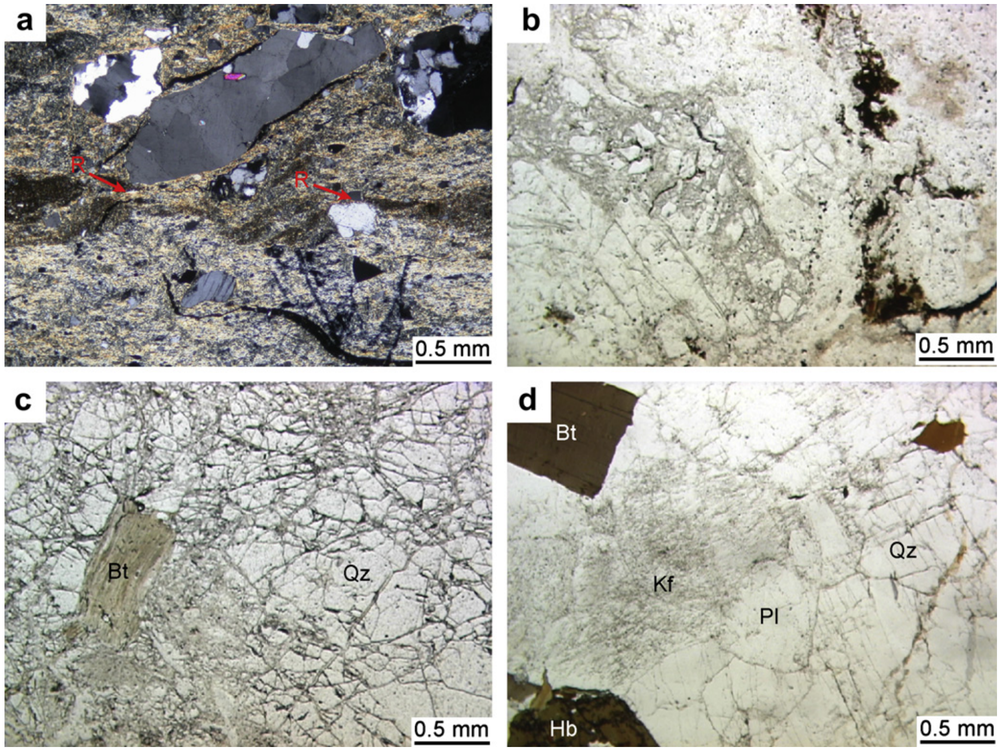

Fig. 3. Microphotographs of greenish–gray clayey gouge (a), fault breccia (b), fractured granite (c), and granite (d) sampled at the Funaki outcrop. Figure (a): crossed-polarized light; (b–d) plane-polarized light. Qz: quartz, Bt: biotite, Kf: alkali feldspar, Pl: plagioclase, Hb: hornblende. Arrows indicate Riedel shear planes.

dark brown clayey gouge of about 0.03–0.1 m in width, gray gouge of about 0.1–0.15 m in width, and blue–gray gouge of about 0.1–0.15 m in width. The thicknesses of the different types of gouge vary along the fault. The colors of the gouges indicate that the brown and dark brown clayey gouges are derived from the sandstone, whereas the gray and blue–gray gouges are derived from the granodiorite.

Foliation in the dark brown clayey gouge is defined by white bands of coarse-grained felsic fragments and the preferred orientation of clay minerals (Fig. 5a). The brown gouge contains a weak foliation defined by black bands within the matrix (Fig. 5b). The host sandstone shows a clast-supported texture, with no visible bedding (Fig. 5c).

Black layers within the gray gouge at the southern part of the trench have been reported to be pseudotachylyte (Otsuki et al., 2003); however, the northern part of the trench contains layers of granitic cataclasite in the gouge rather than black layers. Clasts within the gray gouge are smaller and much less abundant than those in the other gouges (Fig. 5d). The very fine-grained nature of the matrix means that it appears black when viewed under an optical microscope in crossed-polarized light.

In the granitic cataclasite, the original texture of the host rock can be observed at the mesoscopic scale, whereas the original texture can no longer be observed at the microscopic scale (Fig. 5e). A foliation is defined by color banding in the matrix and crushed particles that were aligned during cataclastic flow. Foliation within the blue–gray gouge is defined by thin, elongate layers of opaque minerals in the matrix (Fig. 5f). In the breccia zone, the mesoscopic structure of the host rock is no longer visible, and the texture is typically characterized by large fragments within a fine-grained matrix (Fig. 5g). In the fractured granodiorite, the structure of the host rock is retained, and numerous fractures are filled with finely crushed grains (Fig. 5h).

Samples for permeability measurements were collected from the fault gouge zone, the fault breccia zone, and the fractured granite zone within an excavated trench. In addition, sample GR118 (see Table 1) was collected from a microshear zone in the fractured granodiorite.

4. Experimental procedure

Permeability measurements were conducted on samples of fault gouge, fault breccia, fractured granite, and non-fractured granite collected from the two outcrops. For friable fault rocks, a cylindrical sample was obtained by hammering a copper tube (20 mm internal diameter) or stainless steel tube (25 mm internal diameter) into the outcrop. For hard rocks, a cylindrical sample was cored in the laboratory. Cylindrical axes of all samples we prepared correspond to one of the following three directions. Direction 1 is parallel to the direction of slip upon the fault plane, Direction 2 is parallel to the fault plane and perpendicular to the direction of slip, and Direction 3 is perpendicular to the fault plane. Prior to permeability measurements, the cylindrical samples (20 and 25 mm in diameter and 5–30 mm in length) were dried at 85 °C until constant weight was achieved (the maximum weight loss was 25%).

Table 1
Summary of the results of experiments conducted on fault rocks from the Nojima fault zone where exposed at Funaki and Hirabayashi

Sample	Sampling location	Rock type	Measurement method	P_c [MPa]	P_p [MPa]	Sample orientation	Distance from Fault [m]	Pressurizing path		De-pressurizing path	
								A	B	A	B
GR035*	Funaki	Greenish–gray clayey gouge	OPP	30–110	20	1	0	5.29×10^{-11}	−4.31	1.81×10^{-18}	−0.47
GR049	Funaki	Greenish–gray clayey gouge	OPP	30–50	20	3	0	5.16×10^{-11}	−4.99	–	–
GR061	Funaki	Greenish–gray clayey gouge	OPP	30–80	20	1	0	1.71×10^{-9}	−5.97	6.13×10^{-19}	−0.42
GR064	Funaki	Greenish–gray clayey gouge	OPP	30–200	20	1	0	2.99×10^{-10}	−5.41	–	–
GR043	Funaki	Granitic breccia	OPP	30–200	20	1	0.2	1.98×10^{-12}	−1.62	3.16×10^{-15}	−0.39
GR059	Funaki	Granitic breccia	OPP	30–200	20	1	0.2	1.09×10^{-10}	−2.51	–	–
GR063*	Funaki	Granitic breccia	OPP	30–200	20	1	0.3	1.57×10^{-11}	−1.83	1.98×10^{-14}	−0.62
GR056	Funaki	Breccia matrix	OPP	30–200	20	1	0.8	4.80×10^{-13}	−2.14	1.33×10^{-16}	−0.64
GR062	Funaki	Breccia matrix	OPP	30–200	20	1	0.8	1.26×10^{-11}	−2.31	7.25×10^{-16}	−0.40
GR247	Funaki	Granitic breccia	CFR	5–200	0–2	1	2	1.26×10^{-12}	−1.17	1.95×10^{-14}	−0.53
GR158	Funaki	Fractured granite	OPP	30–200	20	1	3	1.95×10^{-13}	−1.52	2.51×10^{-15}	−0.72
GR377	Funaki	Fractured granite	CFR	5–200	0–2	3	3	6.85×10^{-14}	−1.58	3.02×10^{-15}	−1.08
GR376	Funaki	Fractured granite	CFR	5–200	0–2	–	10	3.26×10^{-13}	−2.16	1.57×10^{-15}	−1.22
GR379	Funaki	Fractured granite	CFR	5–200	0–2	3	10	3.26×10^{-13}	−2.51	3.78×10^{-16}	−1.28
GR065	Funaki	Granite	OPP	30–110	20	–	100	1.34×10^{-18}	−1.06	–	–
GR106	Hirabayashi	Sandstone	OPP	30–200	20	2	0.3	2.32×10^{-11}	−2.40	2.88×10^{-15}	−0.70
GR107	Hirabayashi	Brown gouge	OPP	30–200	20	2	0.2	4.23×10^{-5}	−6.34	2.60×10^{-16}	−1.44
GR160	Hirabayashi	Brown gouge	OPP	30–150	20	2	0.1	3.71×10^{-8}	−5.49	2.33×10^{-16}	−2.23
GR161	Hirabayashi	Dark brown clayey gouge	OPP	30–70	20	2	0.05	1.89×10^{-8}	−5.67	–	–
GR115	Hirabayashi	Blue–gray gouge	OPP	30–200	20	3	0.05	2.79×10^{-9}	−4.54	7.31×10^{-17}	−1.96
GR116	Hirabayashi	Granitic cataclasite	OPP	30–200	20	3	0.1	1.56×10^{-10}	−4.17	1.23×10^{-17}	−1.09
GR108	Hirabayashi	Breccia	OPP	30–199	20	2	0.15	7.89×10^{-11}	−2.21	2.87×10^{-15}	−0.25
GR109	Hirabayashi	Breccia	OPP	30–200	20	2	0.55	1.16×10^{-10}	−2.24	1.00×10^{-14}	−0.42
GR118	Hirabayashi	Fractured granite	OPP	30–200	20	3	3	6.16×10^{-8}	−4.95	3.92×10^{-15}	−1.75

OPP: oscillating pore pressure method; CFR: constant flow rate method; *denotes data for the first pressure cycle.

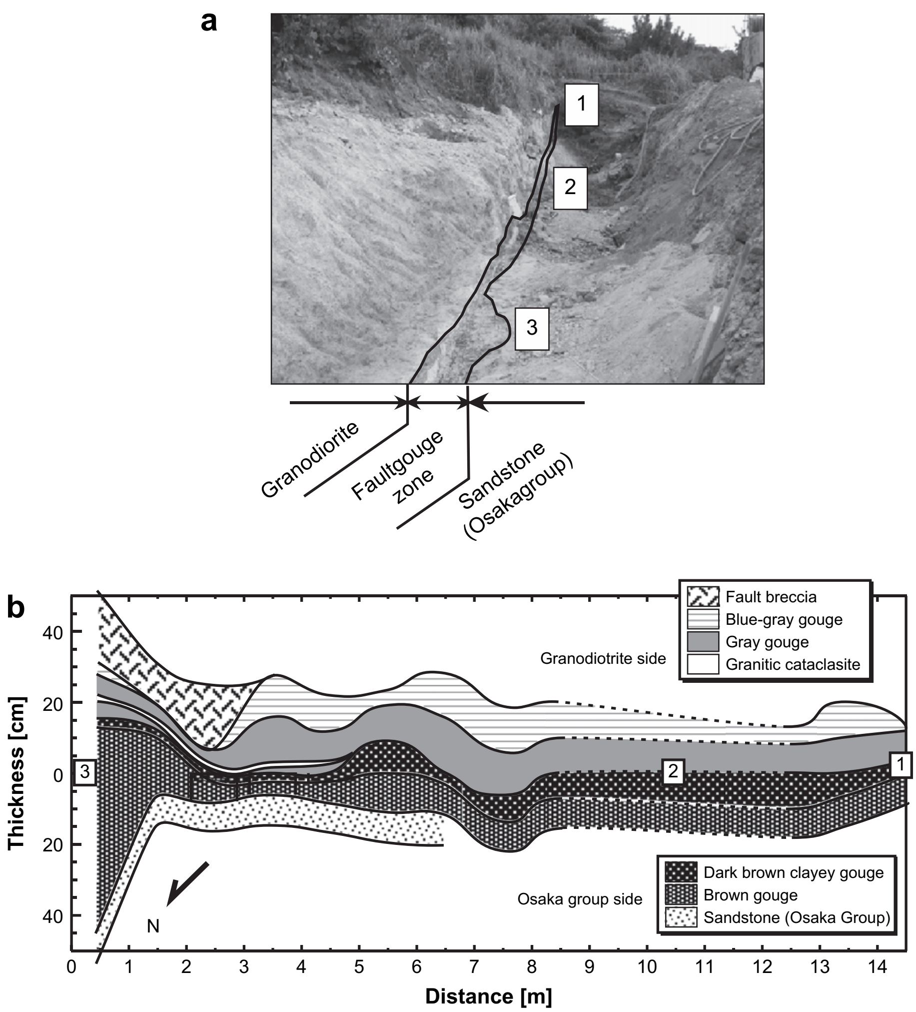

Fig. 4. (a) Photograph of the Hirabayashi outcrop viewed toward the southwest. Numbers 1–3 correspond to the numbered locations in (b). (b) Distribution of fault rocks along the Nojima fault at Hirabayashi.

Experiments were performed using a high-temperature and high-pressure deformation and fluid-flow gas apparatus at Kyoto University, Japan (Fig. 6). In each experiment, a rock sample was placed between the upper and lower pistons, which are equipped with holes to enable the movement of pore fluid into and out of the sample. Porous brass spacers were used to cap the ends of the sample to eliminate flow disturbance at these sites. The sample was jacketed in a heat-shrink polyolefin tube of 2 mm in thickness to separate the pore fluid from the confining medium. Two inlets were used in the confining medium within the pressure vessel (Fig. 6). The confining medium from the lower inlet not only pressurizes the sample but also acts on the upper piston, pushing it upwards. The confining medium counteracts this upward motion by pushing downwards on the upper piston with equal force.

Permeability was measured at room temperature with nitrogen gas as pore fluid and using the flow rate method and oscillating pore pressure method (Kranz et al., 1990; Fischer and Paterson, 1992; ASTM D4525-90, 2001). Pore pressure (P_p) was less than 1 MPa for the former method, and held constant at around 20 MPa for the latter. The confining pressure (P_c) was increased up to 110 MPa for samples with low permeability (gouge and non-fractured granite) and 200 MPa for samples with high permeability (breccia and fractured granite), as the permeability of the former samples at 110 MPa was close to the lower limit (10^{-20}–10^{-19} m^2) of our measurement method.

5. Experimental results

The results obtained for all of the experiments are summarized in Table 1, and Fig. 7 shows the permeabilities of the analyzed samples as a function of effective pressure (P_e). P_e is defined as $P_c - P_p$. The permeabilities showed a rapid decrease as P_e was increased to 180 MPa. Along the de-pressurizing path, the permeabilities showed a slight increase as P_e was reduced from 180 to 50 MPa, and a rapid increase as P_e approached 10 MPa. The values of permeability measured during the de-pressurizing path are consistently lower than those recorded during the pressurizing path. The effective pressure-permeability data obtained during the pressurizing and de-pressurizing paths are well expressed using a power equation, $k = A\,P_e^B$, where k

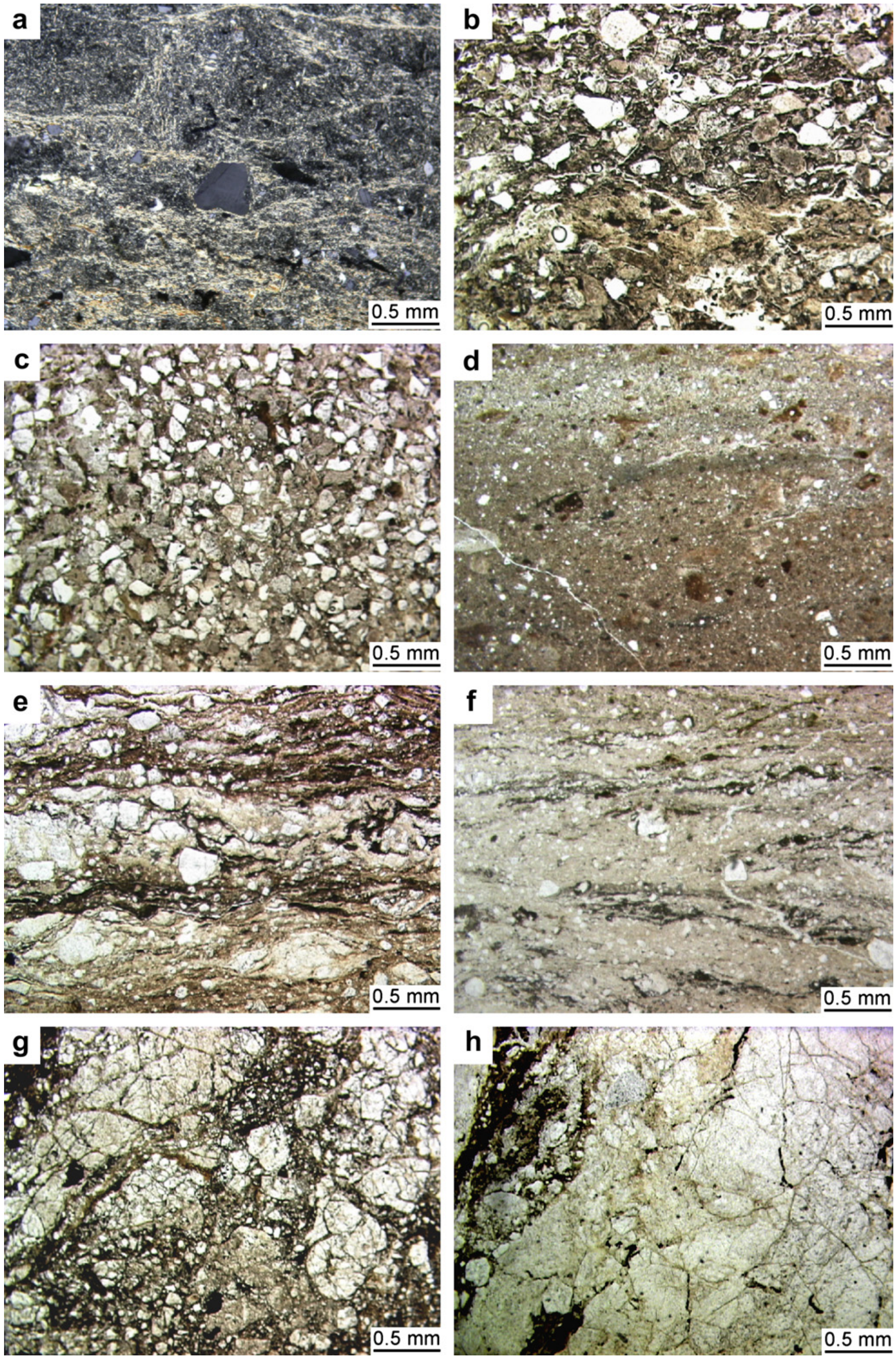

Fig. 5. Microphotographs of dark brown clayey gouge (a), brown gouge (b), sandstone (c), gray gouge (d), granitic cataclasite (e), blue–gray gouge (f), fault breccia (g) and fractured granodiorite (h) sampled at the Hirabayashi outcrop. Figure (a): crossed-polarized light; (b–h) plane-polarized light.

is permeability, A is permeability at $P_e = 0$ MPa, and B is a constant that specifies the rate at which k decreases with increasing P_e (dashed lines in Fig. 7). The calculated values of A and B are listed in Table 1. The experiments revealed similar permeabilities for the samples of fault rock collected from the two outcrops, as described below.

When P_e was increased from 10 to 180 MPa, the permeability of the fault gouge (solid symbols in Figs. 7a,c) decreased more rapidly than that of the other samples by between four and six orders of magnitude, reaching 10^{-20}–10^{-19} m^2 at a P_e value of 180 MPa. The clayey gouges (the greenish–gray clayey gouge and dark brown clayey gouge) have the

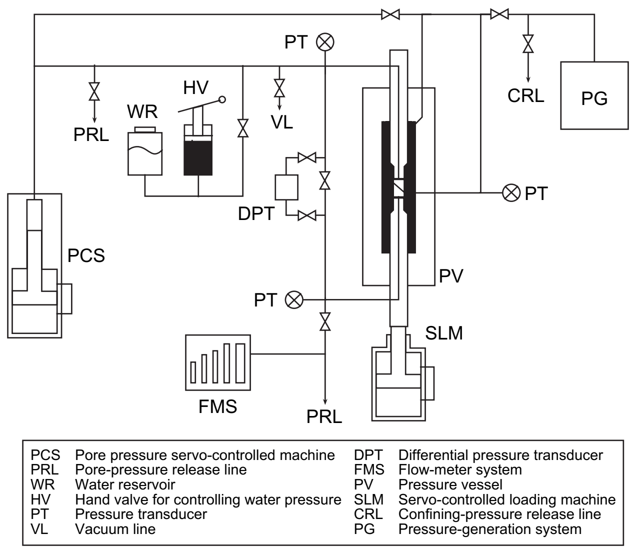

Fig. 6. Simplified diagram of the experimental system employed in the present study. WR, HV, DPT, and SLM were not used in the present permeability tests. FMS is used for measuring the flow rate through the sample, and PCS is used to oscillate the pore pressure in the upstream reservoir.

lowest permeability among the examined gouges (less than 10^{-19} m^2 at $P_e = 80$ MPa).

During de-pressurization, the gouges tended to remember their permeability values at the highest value of P_e. The permeability of the gouges at $P_e = 10$ MPa on the de-pressurizing path was three orders of magnitude lower than that on the hydrostatic loading path. The permeability of sample cored perpendicular to foliation (GR049) was similar to that of samples cored parallel to foliation.

The permeability of the fault breccia (open symbols in Fig. 7a and gray symbols in Fig. 7c) decreased by between one and three orders of magnitude with increasing P_e from 10 to 180 MPa, reaching 10^{-17}–10^{-14} m^2 at $P_e = 180$ MPa. The samples of fault breccia showed greater variation in permeability than the fault gouge samples. For samples collected from the fault breccia zone at Funaki, the granitic breccia was more highly permeable than the breccia matrix.

The permeability of the fractured granite (open symbols in Fig. 7b) was insensitive to pressure, as with the fault breccia, and was 10^{-18}–10^{-16} m^2 at $P_e = 180$ MPa. The samples collected at a distance of 3 m from the fault were more highly permeable than those collected 10 m from the fault. The fractured sample (GR118) recorded similar permeability to the fault gouge samples. Microscopically, sample GR118 is typically matrix-supported, and the structure of the host rock is no longer visible. These observations indicate that the sample was collected from fault gouge within a minor fault that developed in the fractured zone.

Non-fractured granite (solid symbols in Fig. 7b) was insensitive to pressure, and recorded a permeability of 10^{-20} m^2 at $P_e = 90$ MPa. The permeability of the sandstone (open square symbols in Fig. 7c) was also largely insensitive to pressure, and was about 10^{-16} m^2 at $P_e = 180$ MPa.

The permeabilities of the clayey gouge (GR035) and breccia matrix (GR056) were measured over two cycles of

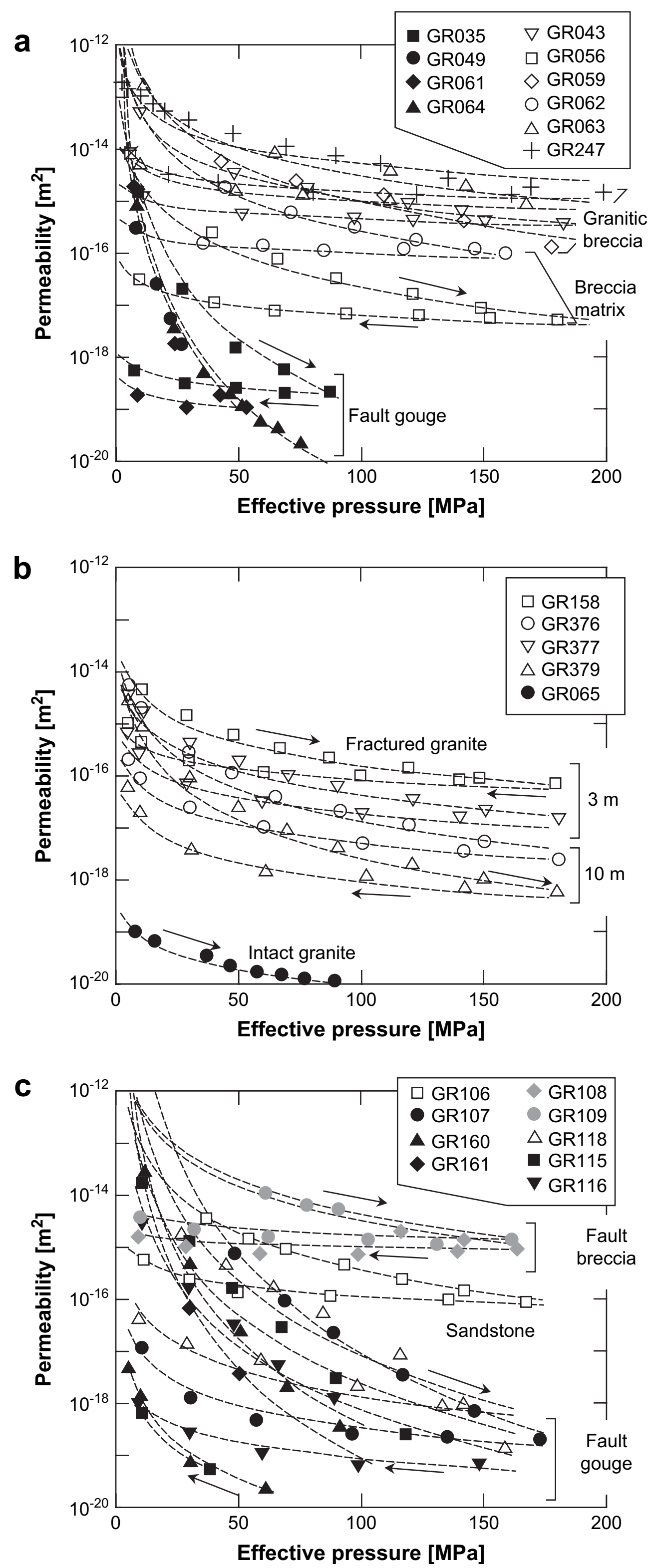

Fig. 7. Permeability of the fault rocks and host rocks collected at Funaki (a and b) and Hirabayashi (c) as a function of effective pressure. Arrows indicate the pressure-cycle path. Dashed lines are least-squares fits (using a power equation) to pressure-dependent permeability data for the pressurizing and de-pressurizing paths.

confining pressure (Fig. 8), revealing little difference in the permeabilities recorded during the first and second deconfining paths. The effect of pressure cycling was therefore not apparent in this test. This result indicates that the samples deformed elasticity after the first peak in confining pressure.

6. Interpretations

6.1. Relationship between microstructure and permeability

Microscopic observations of the three fault-related rock types within the Nojima fault zone—fault gouge, fault breccia, and fractured granite—indicate that each rock type has different types of microcavities, crack and pore, that act as conduits for fluid flow. Intra- and intergranular cracks are predominant in the fractured granite (Fig. 3c), while the fault gouge contains voids, or pores, within the packing framework of mineral grains (Figs. 3a and 5a,b,d–f). The fault breccia contains both cracks within large fragments and pores in the fine-grained matrix (Figs. 3b and 5g).

These two types of microcavities play an important role in controlling fluid flow within fault zones. The present experimental results show that the permeability of the fault gouges decreases with increasing P_e relative to the fault breccia and the fractured granite, even though all three rock types have similarly high permeability at low P_e. This finding indicates that cracks are less sensitive to changes in pressure than pores. Thus, the active pathways of fluid flow throughout the Nojima fault zone consist of both pores and cracks at shallow depths, but cracks alone at greater depth.

6.2. Permeability structure at the surface

The permeability structure of the Nojima fault zone at Funaki is shown in Fig. 9a. The permeability of conglomerate (Osaka Group) exposed in the Funaki trench was not measured because we were unable to collect undisturbed samples. The fault gouge zone and granitic host rock have low permeabilities of less than 10^{-19} m^2, thereby acting as barriers to fluid flow across the fault. This result is consistent with measurements of the permeability of fault gouge samples reported in previous studies (Chu et al., 1981; Morrow et al., 1981, 1984; Faulkner and Rutter, 2000; Wibberley and Shimamoto, 2003). In contrast, the fault breccia zone and fractured granitic host rocks are highly permeable (10^{-18}–10^{-14} m^2), thereby acting as fluid conduits. Thus, the fault zone has an anisotropic permeability structure, with high permeability parallel to the fault and low permeability perpendicular. This finding indicates that fluids tend to migrate parallel to the fault rather than across it, as reported previously for other faults (e.g., Evans et al., 1997; Seront et al., 1998; Wibberley and Shimamoto, 2003; Tsutsumi et al., 2004).

The permeability structure of the Nojima fault at Hirabayashi is shown in Fig. 9b. On the side of the fault that contains Cretaceous granodiorite, the permeability structure of the fault is similar to that at Funaki: the gouge zone has a low permeability whereas the breccia zone and fractured granodiorite zone are highly permeable. This result indicates that the Nojima fault has a consistent permeability structure along its length, although the side of the fault at Hirabayashi that contains rocks of the Osaka Group exhibits a different permeability structure from that on the granodiorite side. This side of the fault contains a fault gouge zone with low permeability, but lacks a relatively permeable breccia or fractured zone. This result, of contrasting permeability structures in the two lithologies, is similar to that reported in previous studies (e.g., Antonellini and Aydin, 1994), raising the possibility that faults developed in sandstone have different permeability structures to those developed in granite.

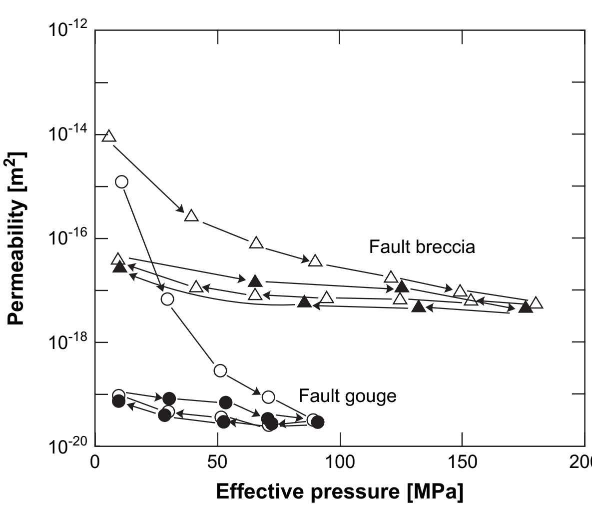

Fig. 8. Permeability data obtained from pressure cycling tests on clayey gouge (GR035, triangles) and breccia matrix (GR056, circles). Permeability is plotted as a function of effective pressure. Open symbols represent the first cycle path, and solid symbols the second.

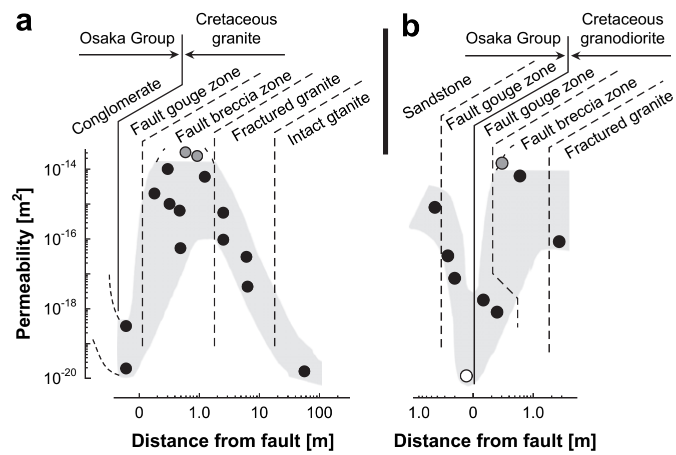

Fig. 9. Permeability structure of the Nojima fault at Funaki (a) and Hirabayashi (b). Permeability at $P_e = 90$ MPa is plotted as a function of distance from the fault trace. The permeabilities of the samples marked by a gray circle were greater than 10^{-14} m^2, and the permeability of the sample marked by an open circle was less than 10^{-20} m^2.

6.3. Comparison of the permeability of surface samples, core samples, and in situ measurements

After the 1995 Kobe earthquake, the Disaster Prevention Research Institute of Kyoto University (DPRI) drilled three boreholes near the Funaki site to depths of 500, 800, and 1800 m. In addition, the National Research Institute for Earth Science and Disaster Prevention (NIED) of Japan and the Geological Survey of Japan (GSJ) drilled boreholes to depths of 1838 and 747 m, respectively, at the Hirabayashi site, close to the central segment of the Nojima fault. The borehole drilled by the GSJ intersected the Nojima fault at a depth of 624 m, and the borehole drilled by NIED intersected deformed zones related to the fault at depths of 1140, 1320, and 1800 m. Where intersected by the boreholes, the fault zone consists of granodiorite in both the footwall and hanging wall, with a narrow clay-rich or fine-grained fault core and a surrounding damage zone of highly fractured rock (Lockner et al., 2000).

They measured the permeability of core samples from both the GSJ and NIED boreholes using water as a pore fluid, obtaining values for the fault core of 10^{-19}–10^{-18} m^2 at $P_e = 50$ MPa. This value is similar to that obtained in the present study for clayey gouge sampled at the surface (greenish–gray clayey gouge at Funaki and dark brown clayey gouge at Hirabayashi). The permeability of the damaged zone at depth is 10^{-17}–10^{-16} m^2 at $P_e = 50$ MPa, similar to our estimate for the fractured granite zone at the surface fault but lower by two orders of magnitude than the permeability of the fault breccia at the surface. It should be noted, however, that the results of Lockner et al. (2000) were obtained using water as a pore fluid, whereas gas was used in the present study. It has been reported that gas permeability is higher than water permeability, and that the maximum difference is an order of magnitude for clay-rich rocks (Brace et al., 1968; Faulkner and Rutter, 2000; Tanikawa and Shimamoto, 2006). Considering the permeability difference associated with the pore fluids employed in the two studies, the lowest and most highly permeable zones at the surface have permeabilities that are an order of magnitude lower and higher than those at depth, respectively.

The permeability structure of the Nojima fault at the surface, consisting of an impermeable zone surrounded by highly permeable zones, is consistent with that estimated at depth. It should be emphasized that the differences in permeability reported in the two studies is within an order of magnitude for each of the zones along the fault, suggesting that the estimate of the permeability structure at the surface is quantitatively consistent with that at depth.

Several previous studies that undertook *in situ* measurements report that the permeability of the Nojima fault zone decreases from approximately 10^{-12} to 10^{-16} m^2 with increasing depth from 0.5 to 3 km (Kitagawa et al., 1999; Kiguchi et al., 2001; Murakami et al., 2001; Tadokoro et al., 2001). Assuming hydrostatic pore pressure, this depth interval corresponds to a range in effective pressure from 10 to 45 MPa. Under these low pressures in the present experiments, we obtained permeability values of 10^{-16}–10^{-13} m^2 for fault breccia and fractured granite zones. Even if the effect of pore fluid is considered, the results of the *in situ* experiments can be explained by fluid flow through the zones of fault breccia and fractured granite.

A comparison of the present results with those obtained previously based on logging data and core samples indicates that the permeability at the surface of the Nojima fault is similar to that at depth. Accordingly, it is possible to estimate the permeability of a fault at depths down to several kilometers based on analyses of samples collected from the surface. This indicates that the surface estimate of the permeability of other faults reported in previous studies (e.g., Evans et al., 1997; Seront et al., 1998; Wibberley and Shimamoto, 2003; Tsutsumi et al., 2004) could be safely extrapolated to depths of up to 2 km.

For the Nojima fault, it might well be possible to discuss spatial variations in the permeability structure of the fault at shallow depths based on data obtained from surface samples; however, it has yet to be determined whether data obtained from surface samples is useful in terms of inferring the permeability of the fault zone to depths within the seismogenic zone (~10 km), which would be relevant to investigations of earthquake generation processes. Should a deep borehole be drilled across a fault in the future, it might be possible to test the depth limitation of data obtained from surface samples in terms of permeability analysis.

6.4. Thermal pressurization upon the Nojima fault

Here, we use the permeability structure obtained in the present study as a basis for examining the possibility that thermal pressurization occurred on the Nojima fault during the Kobe earthquake. We expect that low-permeability fault gouge might prevent water heated by frictional slip from escaping from the gouge zone, thereby leading to an increase in pore pressure, a reduction in shear strength upon the fault, and leading in turn to dynamic weakening in association with a high slip rate.

We consider a one-dimensional fluid- and heat-flow model in the direction perpendicular to the fault. The three parameters that play an important role in the modeling are hydraulic diffusivity (D_h), the thermal pressurization coefficient (Γ), and the characteristic time for thermal pressurization (Ψ):

$$D_h = \frac{\kappa}{\eta\beta_c} \tag{1}$$

$$\Gamma = \frac{\phi\alpha_w + (1-\phi)\alpha_m - \alpha_{sf}}{\beta_c} \tag{2}$$

$$\Psi = \frac{\rho c W_{0.5}}{\mu_d \Gamma \cdot V} \tag{3}$$

where κ is the permeability of the fault gouge, η is the fluid dynamic viscosity, β_c is the storage capacity of the fault gouge, ϕ is the porosity of the fault gouge, α_w is the thermal expansivity of water, α_m is the mineral thermal expansivity, α_{sf} is the thermal expansivity of the porous medium, ρ is the rock density, c is the rock specific heat capacity, $W_{0.5}$ is the half-width of the fault gouge zone, μ_d is the dynamic coefficient of friction, and V is relative slip velocity (Lachenbruch, 1980; Mase and Smith, 1987; Wibberley and Shimamoto, 2005). If the length scale of hydraulic diffusion $L_h = (D_h\Psi)^{1/2}$ is less than $W_{0.5}$, we can assume that fluid loss from the gouge zone is negligible at the time scale of earthquake rupture when heat is generated (Wibberley and Shimamoto, 2005). In the case of no fluid loss, the shear resistive stress (τ) decreases exponentially due to thermal pressurization:

$$\tau = \mu_d(\sigma_n - p_i)\exp\left(-\frac{d}{V\Psi}\right) \quad (4)$$

where σ_n is the normal stress on the fault, p_i is the initial pore pressure, and d is the displacement. Using the values shown in Table 2, we found that the condition $L_h < W_{0.5}$ is satisfied when $\kappa < 4.78 \times 10^{-16}\ m^2$.

Applying the above relation to the permeability data obtained for the Nojima fault in the present study, thermal pressurization occurs provided that P_e exceeds 60 MPa. This condition corresponds to the ambient pressure at a depth of 4 km, assuming gradients in lithostatic and fluid pressure of 25 and 10 MPa/km, respectively. This finding indicates that thermal pressurization could have occurred during the 1995 Kobe earthquake at depths greater than 4 km. The slip models proposed for the Kobe earthquake (e.g., Ide and Takeo, 1997) show major slip at depths shallower than 5 km. This suggests that a component of the large slip that occurred at shallow depths was related to a weakening mechanism other than thermal pressurization, such as the ‘‘high-velocity gouge weakening’’ that has been documented in friction tests on the Nojima fault gouge (blue–gray gouge in this paper) at seismic slip rates under lower-than-normal stress condition of less than 1.85 MPa (Mizoguchi et al., 2007).

Table 2
Parameter values employed for analyses of thermal pressurization

Property	Value
Storage capacity[b], β_c	$1 \times 10^{-10}\ Pa^{-1}$
Porosity[c], ϕ	0.3
Rock density[a], ρ	$2600\ kg\ m^{-3}$
Rock heat capacity[a], c	$1000\ J\ kg^{-1}\ K^{-1}$
Water viscosity[a], η	2.89×10^{-4} Pa s
Water expansivity[a], α_w	$6.24 \times 10^{-4}\ K^{-1}$
Mineral expansivity[a], α_m	$2 \times 10^{-5}\ K^{-1}$
Porous medium expansivity[a], α_{sf}	$1 \times 10^{-5}\ K^{-1}$
Half-width of the gouge zone, $W_{0.5}$	0.075 m
Dynamic coefficient of friction, μ_d	0.6
Slip velocity[d], V	$0.5\ m\ s^{-1}$

[a] Values are taken from Wibberley and Shimamoto (2005).
[b] β_c is assumed to be constant with changing pressure based on the findings of Wibberley and Shimamoto (2005).
[c] The porosity value was obtained from Aizawa et al. (manuscript in preparation, 2007).
[d] Waveform inversion by Ide and Takeo (1997) showed that the slip velocity on the Nojima fault during the 1995 Kobe earthquake reached a maximum of 0.5 m/s.

7. Conclusions

We measured the permeability of samples taken from a fault gouge zone, a fault breccia zone, and a fractured granite zone along the Nojima fault at Funai and Hirabayashi under isotropic confining pressures of up to 180 MPa. The fault gouge records the lowest permeability (10^{-20}–$10^{-19}\ m^2$ at 180 MPa), thereby acting as a barrier to fluid flow across the fault; in contrast, breccia and fractured host rocks are highly permeable (10^{-18}–$10^{-14}\ m^2$ at 180 MPa), acting as fluid conduits. These permeabilities obtained for surface samples of fault rock are largely consistent with those obtained for borehole samples collected at 2 km depth. We therefore propose that permeability data obtained from surface samples collected along other faults in addition to the Nojima fault can be used to infer their permeability structures to depths of up to 2 km. Based on the assumption that the present experimental results regarding fault permeability can be extrapolated to depth, we note that thermal pressurization might have occurred on the Nojima fault at depths greater than 4 km during the 1995 Kobe earthquake.

Acknowledgements

The authors are grateful to Akito Tsutsumi, Shin-ichi Uehara, Christopher A.J. Wibberley, and Keiji Sato for valuable discussions and critical readings of the manuscript. The authors also wish to thank Professor Kenshiro Otsuki for providing the samples analyzed in the present experiments. The manuscript greatly benefited from thoughtful reviews by Andrea Bizzarri and an anonymous reviewer.

References

Antonellini, M., Aydin, A., 1994. Effect of faulting on fluid flow in porous sandstones: petrophysical properties. AAPG Bulletin 78, 355–377.
ASTM D4525-90, 2001. Standard Test Method for Permeability of Rocks by Flowing Air. ASTM International, West Conshohocken.
Awata, Y., Mizuno, K., 1998. Explanatory text of the strip map of the surface fault rupture associated with the 1995 Hyogo-ken Nanbu Earthquake, Central Japan. Tectonic Map Series 12, Geological Survey of Japan.
Bizzarri, A., Cocco, M., 2006a. A thermal pressurization model for the spontaneous dynamic rupture propagation on a three-dimensional fault: 1. Methodological approach. Journal of Geophysical Research 111, B05303, doi:10.1029/2005JB003862.
Bizzarri, A., Cocco, M., 2006b. A thermal pressurization model for the spontaneous dynamic rupture propagation on a three-dimensional fault: 2. Traction evolution and dynamic parameters. Journal of Geophysical Research 111, B05304, doi:10.1029/2005JB003864.
Brace, W.F., Walsh, J.B., Frangos, W.T., 1968. Permeability of granite under high pressure. Journal of Geophysical Research 73, 2225–2236.
Caine, J.S., Evans, J.P., Forster, C.B., 1996. Fault zone architecture and permeability structure. Geology 24, 1025–1028.
Chu, C.L., Wang, C.Y., Lin, W., 1981. Permeability and frictional properties of San Andreas Fault gouges. Geophysical Research Letters 8, 565–568.
Evans, J.P., Forster, C.B., Goddard, J.V., 1997. Permeability of fault-related rocks, and implications for hydraulic structure of fault zone. Journal of Structural Geology 19, 1393–1404.
Faulkner, D.R., Rutter, E.H., 2000. Comparison of water and argon permeability in natural clay-bearing fault gouge under high pressure at 20 °C. Journal of Geophysical Research 105, 16415–16427.

Fischer, G.J., Paterson, M.S., 1992. Measurement of permeability and storage capacity in rocks during deformation at high temperature and pressure. In: Evans, B., Wong, T.-F. (Eds.), Fault Mechanics and Transport Properties of Rocks. Academic Press, New York, pp. 187–211.

Healy, J.H., Rubey, W.W., Griggs, D.T., Raleigh, C.B., 1968. The Denver Earthquakes: Disposal of waste fluids by injection into a deep well has triggered earthquakes near Denver, Colorado. Science 161, 1301–1310.

Huzita, K., 1967. Quaternary crustal movements in the "Kinki Triangle", Southwest Japan. Journal of Geosciences, Osaka City University 10, 21–23.

Huzita, K., 1969. Tectonic development of Southwest Japan in the Quaternary Period. Journal of Geosciences, Osaka City University 12, 53–70.

Ide, S., Takeo, M., 1997. Determination of constitutive relations of fault slip based on seismic wave analysis. Journal of Geophysical Research 102, 27379–27391.

Kiguchi, T., Ito, H., Kuwahara, Y., Miyazaki, T., 2001. Estimating the permeability of the Nojima Fault Zone by a hydrophone vertical seismic profiling experiment. The Island Arc 10, 348–356.

Kitagawa, Y., Koizumi, N., Notsu, K., Igarashi, G., 1999. Water injection experiments and discharge changes at the Nojima fault in Awaji Island, Japan. Geophysical Research Letters 20, 3173–3176.

Kranz, R.L., Saltzman, J.S., Blacic, J.D., 1990. Hydraulic diffusivity measurements on laboratory rock samples using an oscillating pore pressure method. International Journal of Rock Mechanics, Mineral Science and Geomechanical Abstracts 27, 345–352.

Lachenbruch, A.H., 1980. Frictional heating, fluid pressure, and the resistance to fault motion. Journal of Geophysical Research 85, 6097–6112.

Lockner, D.A., Naka, H., Tanaka, H., Ito, H., Ikeda, R., 2000. Permeability and strength of core samples from the Nojima fault of the 1995 Kobe earthquake. In: GSJ Internal Report No. EQ/00/1, Proceedings of the Internal Workshop on Nojima Fault Core and Borehole Date Analysis, pp. 147–157.

Mase, C.W., Smith, L., 1985. Pore-fluid pressures and frictional heating on a fault surface. Pure and Applied Geophysics 122, 583–607.

Mase, C.W., Smith, L., 1987. Effects of frictional heating on the thermal, hydrologic, and mechanical response of a fault. Journal of Geophysical Research 92, 6249–6272.

Mizoguchi, K., Hirose, T., Shimamoto, T., Fukuyama, E., 2007. Reconstruction of seismic faulting by high-velocity friction experiments: an example of the 1995 Kobe earthquake. Geophysical Research Letters 34, L01308, doi:10.1029/2006GL027931.

Mizuno, K., Hattori, H., Sangawa, A., Takahashi, Y., 1990. Geology of the Akashi District. With Geological Sheet Map at 1:50,000, Geological Survey of Japan.

Morrow, C.A., Lockner, D.A., 1994. Permeability differences between surface-derived and deep drillhole core samples. Geophysical Research Letters 21, 2151–2154.

Morrow, C.A., Shi, L.Q., Byerlee, J.B., 1981. Permeability and strength of San Andreas fault gouge under high pressure. Geophysical Research Letters 8, 325–328.

Morrow, C.A., Shi, L.Q., Byerlee, J.B., 1984. Permeability of fault gouge under confining pressure and shear stress. Journal of Geophysical Research 89, 3193–3200.

Murakami, H., Hashimoto, T., Oshiman, N., Yamaguchi, S., Honkura, Y., Sumitomo, N., 2001. Electrokinetic phenomena associated with a water injection experiment at the Nojima fault on Awaji Island, Japan. The Island Arc 10, 244–251.

Murata, A., Takemura, K., Miyata, T., Lin, A., 1998. Vertical displacement and geological cross-section reconstructed from core samples of 500 m hole of Nojima fault. Gekkanchikyu-Gougai 21, 137–143 (in Japanese).

Noda, H., Shimamoto, T., 2005. Thermal pressurization and slip-weakening distance of a fault: An example of the Hanaore Fault, Southwest Japan. Bulletin of the Seismological Society of America 95, 1224–1233.

Ohtake, M., 1974. Seismic activity induced by water injection at Matsushiro, Japan. Journal of Physics of the Earth 22, 163–176.

Otsuki, K., Monzawa, N., Nagase, T., 2003. Fluidization and melting of fault gouge during seismic slip: Identification in the Nojima fault zone and implications for focal earthquake mechanisms. Journal of Geophysical Research 108 (B4), 2192, doi:10.1029/2001JB001711.

Rice, J.R., 2006. Heating and weakening of faults during earthquake slip. Journal of Geophysical Research 111, B05311, doi:10.1029/2005JB004006.

Schön, J.H., 1996. Physical Properties of Rocks: Fundamentals and Principles of Petrophysics. In: Handbook of Geophysical Exploration, vol. 8. Pergamon Press, London.

Seront, S., Wong, T.-F., Caine, J.S., Forster, C.B., Bruhn, R.L., Fredrich, J.T., 1998. Laboratory characterization of hydromechanical properties of a seismogenic normal fault system. Journal of structural geology 20, 865–881.

Sibson, R.H., 1973. Interactions between temperature and fluid pressure during earthquake faulting and a mechanism for partial or total stress relief. Nature 243, 66–68.

Tadokoro, K., Nishigami, K., Ando, M., Hirata, N., Iidaka, T., Hashida, Y., Shimazaki, K., Ohmi, S., Kano, Y., Koizumi, M., Matsuo, S., Wada, H., 2001. Seismicity changes related to a water injection experiment in the Nojima Fault Zone. The Island Arc 10, 235–243.

Tanikawa, W., Shimamoto, T., 2006. Klinkenberg effect for gas permeability and its comparison to water permeability for porous sedimentary rocks. Hydrology and Earth System Sciences Discussions 3, 1315–1338.

Tsutsumi, A., Nishino, S., Mizoguchi, K., Hirose, T., Uehara, S., Sato, K., Tanikawa, W., Shimamoto, T., 2004. Principal fault zone width and permeability of the active Neodani fault, Nobi active fault system, Southwest Japan. Tectonophysics 379, 93–108.

Uehara, S., Shimamoto, T., 2004. Gas permeability evolution of cataclasite and fault gouge in triaxial compression and implications for changes in fault-zone permeability structure through the earthquake cycle. Tectonophysics 378, 183–195.

Wibberley, C.A.J., Shimamoto, T., 2003. Internal structure and permeability of major fault zones: the Median Tectonic Line in Mie Prefecture, Southwest Japan. Journal of Structural Geology 25, 59–78.

Wibberley, C.A.J., Shimamoto, T., 2005. Earthquake slip weakening and asperities explained by thermal pressurization. Nature 436, 689–692.

Zoback, M.D., Harjes, H.-P., 1997. Injection-induced earthquakes and crustal stress at 9 km depth at the KTB deep drilling site, Germany. Journal of Geophysical Research 102, 18477–18491.